Contract No.:

This manuscript has been authored by Savannah River Nuclear Solutions (SRNS), LLC under Contract No. DE-AC09-08SR22470 with the U.S. Department of Energy (DOE) Office of Environmental Management (EM).

Disclaimer:

Remotely Detected Vehicle Mass from Suspension Response to an Impulse

Troy R. McKay[a], **Carl Salvaggio**[a], **Jason W. Faulring**[a], **Glenn D. Sweeney**[a]
[a]Rochester Institute of Technology, Digital Imaging and Remote Sensing Laboratory, Chester F. Carlson Center for Imaging Science, College of Science, Rochester, New York, USA, 14623

Abstract.
A method to remotely measure the mass of a vehicle could improve traffic safety by reducing the number of overloaded vehicles on the road. This work presents a method of calculating the mass of a vehicle using ground-based video measurements. The method uses innovative video tracking algorithms to measure the position of the vehicle as it travels over a speed bump, and the response of its suspension system. These position and suspension response measurements, combined with a physics-based vehicle suspension model are used to calculate the mass and position of the vehicle's load. The model consists of a system of second-order differential equations which describe the response of two rigidly-coupled damped-harmonic oscillators to an input signal. The output of the model is the mass and center of gravity of the load being carried by the vehicle, given that the suspension parameters (spring constants and damping coefficients), and unloaded vehicle parameters (unloaded mass, center of gravity, and moment of inertia) are known. This method was tested using an unloaded, half-loaded, and fully-loaded passenger vehicle. The results showed good agreement between the calculated mass and center of gravity and their true values.

Keywords: video tracking, vehicle mass, vehicle suspension, mass prediction, automated monitoring.

*Troy McKay, troy@hyperspectralsolutions.com

1 Introduction

Overloaded vehicles increase the risk of accidents and cause premature deterioration of roads and bridges. When a vehicle is loaded in excess of their maximum recommended limit, they can become less stable due to an elevated center of gravity which can over-strain the on-board stability systems, increasing the potential for rollover accidents and jack-knifing.[1] The braking capacity can be significantly reduced due to overloading causing increased braking distance.[1] Other risks associated with the operation of overloaded vehicles include an increased chance of a tire blowout, and a higher likelihood of a brake fire.[1] Overloaded vehicles also cause accelerated wear to roads and bridges. The relationship between vehicle weight and pavement damage has been shown to be exponential.[2] Bridges can experience increased fatigue damage due to continued exposure this repeated load.[1]

Traditionally, only large trucks are subjected to overloading enforcement. This enforcement is carried out by the random weighing of trucks at static weigh stations.[3] The trucks are driven onto scales and drivers of overloaded trucks are subjected to substantial fines. This method requires the presence of a staff and it takes significant time to weigh the truck and issue the citation to the driver.[1] As a result not all trucks are weighed, which leads to more drivers pushing the limits and driving overloaded. A method of measuring the mass of a vehicle using a ground-based, real-time, imaging system would increase efficiency and allow overloaded vehicles to be identified and singled out. This would reduce the costs associated with manning a weigh station, allow appropriately-loaded vehicles to avoid unwarranted delays, and protect the public from the dangers presented by these overloaded vehicles. This paper presents a method for calculating the mass of a vehicle remotely using ground-based imagery.

2 Methodology

The method described in this paper uses a physics-based model of the vehicle's suspension to simulate the response of the suspension to an impediment (speed bump) for a range of vehicle load masses and center of gravity locations. These simulated responses are compared to the measured response of the vehicle to solve for the mass and center of gravity of the load. There are three critical aspects to this method, the physics-based suspension model, the frame-position tracking algorithm, and the wheel-tracking algorithm. This section will describe, in detail, these three critical aspects.

2.1 Physics-Based Suspension Model

To model the suspension, the vehicle will be approximated as a rigid body, supported by two damped springs (a simple passenger vehicle). Excitation will be introduced to the model as the vertical position of each of the vehicle's axles. The model will be governed by a balance of forces equation, and a balance of torques equation that will be combined to define the position and orientation of the vehicle frame at all times.

When a vehicle travels over a speed bump, the suspension responds; the springs stretch and compress linearly in response to applied forces, and the dampers resist motion. The force applied by each spring and damper can be described using the following equations

$$F_s = k_s \cdot y \tag{1}$$

$$F_d = k_d \cdot \frac{dy}{dt} \tag{2}$$

where F_s is the force applied by the spring, F_d is the force applied by the damper, k_s is the spring constant, k_d is the damping coefficient, and y is the deflection of the spring from its equilibrium position. For a two-axle vehicle traveling over a speed bump, each axle can be modeled individually using the following balance of forces equation

$$m\frac{d^2y}{dt^2} - k_d\frac{dy}{dt} - k_s \cdot y + g \cdot m = 0 \tag{3}$$

where m is the mass supported by the axle, and g is the acceleration due to gravity. In this expression, the spring constant represents the total spring constant for the axle (usually consisting of two

springs). The same is true for the damping coefficient.

To model the suspension of a two-axle vehicle, the front and rear axle need to be coupled by the vehicle frame, and a method of introducing energy into the system must be defined. A diagram of the suspension response model for a typical two-axle vehicle can be seen in Figure 1. In this diagram, y_{A1} and y_{A2} are the vertical positions of the vehicle axles. These vertical positions are defined to be equal to zero when the vehicle is traveling on flat road. A positive value for y_{A1} or y_{A2} would indicate a rise in the road as shown in Figure 2. The terms y_{F1} and y_{F2} are defined as the vertical positions of the vehicle frame at the points where the suspension is joined to the frame (front and rear, respectively). For simplicity, these vertical positions are defined to be equal to zero when the vehicle is traveling on flat road and the suspension spring is in an uncompressed state as shown in Figure 3. When any load is added to the system, the springs compress, resulting in negative values for y_{F1} and y_{F2}. The deviation of the front suspension spring from its uncompressed state can be calculated by subtracting y_{A1} from y_{F1}. Likewise, the deviation of the rear suspension spring from its uncompressed state can be calculated by subtracting y_{A2} from y_{F2}. A positive spring length represents a stretched spring, while a negative spring length represents a compressed spring. The term y_{cg} is defined as the vertical position of the vehicle frame at its center of gravity, and can be thought of as lying on a line connecting points y_{F1} and y_{F2} at a distance x_{cg} from y_{F1}. The variable d is defined as the distance between the point where the front and rear suspensions are joined to the frame (this constant value can be assumed to be the distance between the center of the front and rear axle). The term θ is the angle that the line connecting points y_{F1} and y_{F2} creates from horizontal. The variables F_1, F_{cg}, and F_2 are the forces acting on the vehicle's frame due to the front suspension, gravity, and the rear suspension, respectively. In this simplified model it is assumed that forces F_1, F_{cg}, and F_2 all act perpendicular to the flat

ground.

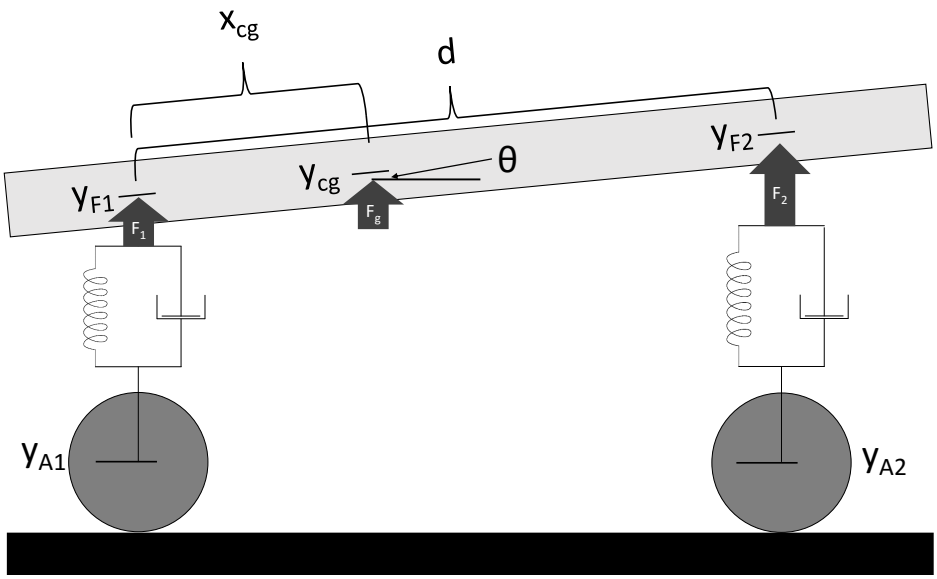

Fig 1: Simplified suspension diagram for a standard two-axle vehicle

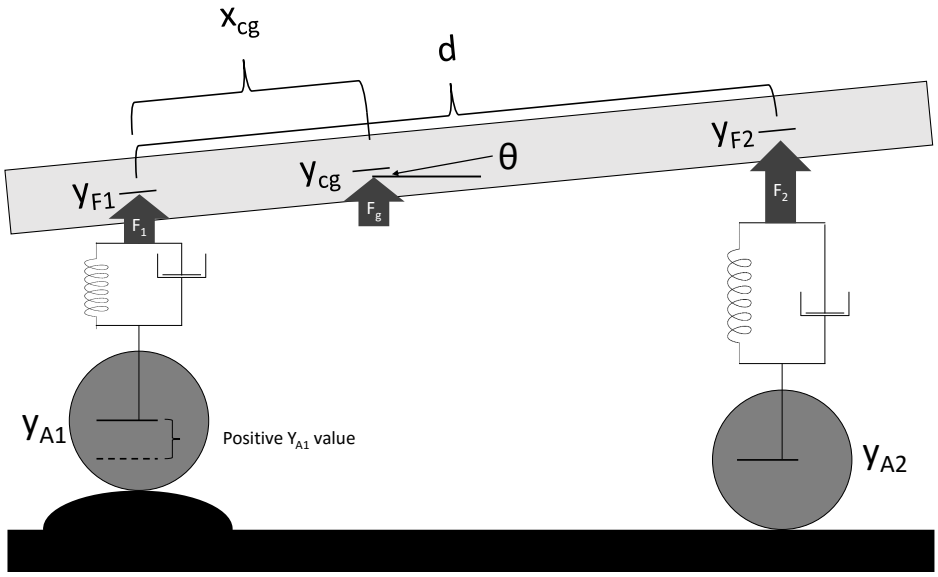

Fig 2: Example of the front axle traveling over a rise in the road (speed bump)

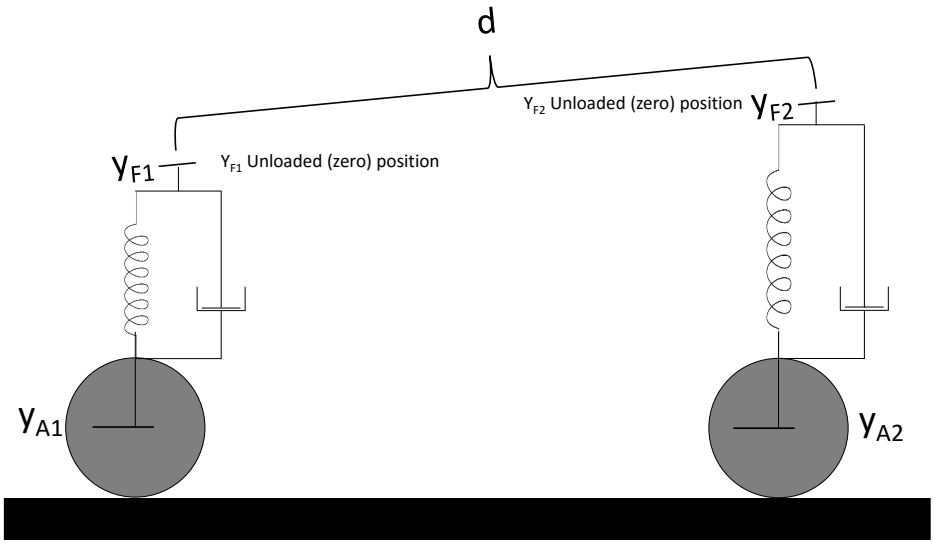

Fig 3: Example of the completely unloaded vehicle traveling over flat road (both springs are in the uncompressed state)

The vehicle frame position can be described completely with only the vertical position of the point on the frame where the front suspension is joined, y_{F1}, and the angle of the frame, θ. The vertical position of any point on the line connecting y_{F1} and y_{F2} can be described as a function of y_{F1} and θ.

$$y_{F2} = y_{F1} + d \cdot \sin(\theta) \tag{4}$$

$$y_{cg} = y_{F1} + x_{cg} \cdot \sin(\theta) \tag{5}$$

For simplification, the small angle approximation ($\sin(\theta) = \theta$) will be used in Equations 4 and 5.

For this model, forces can only be applied at three locations (identified in Figure 1); above each axle, and at the center of gravity of the vehicle frame (located a distance of x_{cg} away from the front axle). The force applied at the front axle, F_1, is applied by the front suspension, the force applied

at the rear axle, F_2, is applied by the rear suspension, and the force applied at the center of gravity, F_g, is the force due to gravity as shown in the following equations

$$F_1 = k_{s1}\left(y_{A1} - y_{F1}\right) + k_{d1}\left(\dot{y_{A1}} - \dot{y_{F1}}\right) \tag{6}$$

$$F_2 = k_{s2}\left(y_{A2} - y_{F2}\right) + k_{d2}\left(\dot{y_{A2}} - \dot{y_{F2}}\right) \tag{7}$$

$$F_g = m \cdot g \tag{8}$$

where k_{s1} and k_{s2} are the spring constants of the front and rear suspension; k_{d1} and k_{d2} are the damping coefficients of the front and rear suspension, respectively, and m is the total mass of the vehicle frame and load.

For this model, torque will be considered about the center of gravity of the vehicle frame. The torques are defined as, τ_1, the torque applied by the front suspension, τ_2, the torque applied by the rear suspension, and τ_g, the torque applied by the force of gravity.

$$\tau_1 = -F_1 \cdot x_{cg} \tag{9}$$

$$\tau_2 = F_2 \cdot (d - x_{cg}) \tag{10}$$

$$\tau_g = F_g \cdot 0 = 0 \tag{11}$$

Now that the forces and torques have been defined, the balance of forces and balance of torques equations can be expressed. Equation 12 defines the vertical acceleration of the center of gravity of the frame as a function of the total mass of the vehicle frame and load, and the three forces acting on it. Equation 13 defines the angular acceleration of the vehicle frame about its center of gravity as a function of the rotational inertia of the vehicle frame, and the two non-zero torques acting on it.

$$\ddot{y_{cg}} \cdot m = F_1 + F_2 + F_g \tag{12}$$

$$\ddot{\theta} \cdot J = \tau_1 + \tau_2 \tag{13}$$

By combining Equations 4, 5 6, 7, 8, and 12, the balance of forces equation can be used to express the vertical acceleration of the frame and load's center of gravity in terms of the suspension parameters (k_{s1}, k_{s2}, k_{d1}, k_{d2}), the vertical position of the vehicle frame at the point where the front suspension is joined (y_{F1}), the vertical position of the front and rear axles (y_{A1} and y_{A2}), the angle of the frame (θ), the distance of the center of gravity of the vehicle from the front axle (x_{cg}), the mass of the vehicle (m), and the acceleration due to gravity (g).

Similarly, by combining Equations 4, 6, 7, 9, 10, and 13, the balance of torques equation can be used to express the angular acceleration of the frame about the center of gravity in terms of the suspension parameters (k_{s1}, k_{s2}, k_{d1}, k_{d2}), the vertical position of the vehicle frame at the point where the front suspension is joined (y_{F1}), the vertical position of the front and rear axles (y_{A1} and y_{A2}), the angle of the frame (θ), the acceleration due to gravity (g), the distance of the center of gravity of the vehicle from the front axle (x_{cg}), and the rotational inertia of the vehicle frame (J).

The balance of forces and balance of torques equations taken together, make up a system of differential equations with two-dependent variables, $y_{F1}(t)$ and $\theta(t)$. If the system parameters, and initial conditions are known, this system of differential equations can be solved for any given road profile to simulate the suspension response as a function of time. The suspension parameters can be estimated by vehicle type, and the road profile can be measured by tracking the vertical position of the center of the vehicle axles. However, measuring the frame position and orientation is more complicated. Even if the vehicle is traveling over flat road and experiencing no suspension bounce the suspensions are still in equilibrium with the force of gravity. This means that the vehicle frame position and orientation can only be measured relative to the static equilibrium position and orientation. This measurement must be corrected by an offset equal to the static equilibrium position and orientation. Fortunately, the static equilibrium position, y_{F1_0}, and orientation, θ_0, can be calculated as a function of the system parameters using Equations 14 and 15.

$$y_{F1_0} = \frac{g \cdot m\,(d - x_{cg})}{d \cdot k_{s1}} \tag{14}$$

$$\theta_0 = \frac{g \cdot m\,(x_{cg}\,(k_{s1} + k_{s2}) - d \cdot k_{s2})}{d^2 \cdot k_{s1} \cdot k_{s2}} \tag{15}$$

These equations for the static equilibrium position and orientation of the frame can be used to correct the measured frame position and orientation, resulting in the absolute frame position and orientation $y_{F1}(t)$ and $\theta(t)$ as shown in the following equations

$$y_{F1}(t) = y_{M1}(t) + y_{F1_0} \tag{16}$$

$$\theta(t) = \theta_M(t) + \theta_0 \tag{17}$$

where $y_{M1}(t)$ is the measured position of the frame above the front axle relative to the static equilibrium position and $\theta_M(t)$ is the measured angular orientation of the frame relative to the static equilibrium orientation. The system of differential equations can now be expressed in terms of measurable values and suspension parameters.

$$\begin{aligned} 0 \;=\; & m\left(x_{cg}\cdot\ddot{\theta_M} + \ddot{y_{M1}}\right) + k_{s1}\left(y_{M1} - y_{A1}\right) + k_{s2}\left(y_{M1} - y_{A2} + d\cdot\theta_M\right) \\ & + k_{d1}\left(\dot{y_{M1}} - \dot{y_{A1}}\right) + k_{d2}\left(\dot{y_{M1}} - \dot{y_{A2}} + d\cdot\dot{\theta_M}\right) \end{aligned} \tag{18}$$

$$\begin{aligned} 0 \;=\; & J\cdot\ddot{\theta_M} + k_{s1}\cdot x_{cg}\left(y_{A1} - y_{M1}\right) \\ & + k_{s2}\left(y_{A2}\cdot x_{cg} - y_{M1}\cdot x_{cg} - d\cdot y_{A2} + d\cdot y_{M1} + d^2\cdot\theta_M - d\cdot\theta_M\cdot x_{cg}\right) \\ & + k_{d1}\left(x_{cg}\cdot\dot{y_{A1}} - x_{cg}\cdot\dot{y_{M1}}\right) \\ & + k_{d2}\left(x_{cg}\cdot\dot{y_{A2}} - x_{cg}\cdot\dot{y_{M1}} - d\cdot\dot{y_{A2}} + d\cdot\dot{y_{M1}} + d^2\cdot\dot{\theta_M} - d\cdot x_{cg}\cdot\dot{\theta_M}\right) \end{aligned} \tag{19}$$

Solving Equation 19 for the angular acceleration ($\ddot{\theta_M}$) results in one of the required ordinary differential equations. Substituting the result into Equation 18 and solving it for the vertical acceleration of the front of the frame ($\ddot{y_{M1}}$) results in the other. These equations for $\ddot{\theta_M}$ and $\ddot{y_{M1}}$ make up the system of differential equations that can be used to model the position and orientation of the frame

as a function of time for a given set of inputs. The measured, estimated, and unknown parameters from the system of differential equations are listed in Table 1.

Table 1: The measured, estimated, and unknown parameters in the initial system of differential equations

Measured Values	**Estimated Parameters**	**Unknown Parameters**
$y_{M1}(t) \quad [m]$	$k_{s1} \quad [N/m]$	$m \quad [kg]$
$\theta_M(t) \quad [rad]$	$k_{d1} \quad [Ns/m]$	$x_{cg} \quad [m]$
$y_{A1}(t) \quad [m]$	$k_{s2} \quad [N/m]$	$J \quad [kg \cdot m^2]$
$y_{A2}(t) \quad [m]$	$k_{d2} \quad [Ns/m^2]$	
$d \quad [m]$		

However, the unknown values defined above; m, x_{cg}, and J are not technically the terms of interest. The main value of interest is the mass of the vehicle's load (m_L), not the total mass of the vehicle frame and load (m). Assuming that the unloaded mass of the vehicle frame, m_0 is known we can express the total mass of the vehicle, m, is simply the sum of the mass of the unloaded vehicle frame, and the mass of the load.

$$m = m_0 + m_L \tag{20}$$

If the center of gravity of the unloaded vehicle frame (x_0) is known, and if both the unloaded vehicle frame and the load are approximated as rigidly coupled point masses, the position of the combined center of gravity, x_{cg}, can be calculated using the following equation

$$x_{cg} = \frac{m_0 \cdot x_0 + m_L \cdot x_L}{m_0 + m_L} \tag{21}$$

where x_0 is the x-axis center of gravity location of the unloaded vehicle, and x_L is the x-axis center of gravity location of the vehicle's load.

The rotational inertia of the loaded vehicle about its center of gravity, J, can be approximated as the sum of the rotational inertias of the unloaded vehicle and the load about the center of gravity, x_{cg}, of the total.

$$J = m_0 \left(x_{cg} - x_0\right)^2 + m_L \left(x_{cg} - x_L\right)^2 \tag{22}$$

Substituting Equation 21 into Equation 22 results in

$$J = \frac{m_0 \cdot m_L \left(x_0 - x_L\right)^2}{m_0 + m_L} \tag{23}$$

Now, as shown in Equations 20, 21, and 23 the three unknown values; m, x_{cg} and J can be expressed in terms of only two unknown values; m_L and x_L. Substituting these into the system of differential equations derived from Equations 18 and 19 produces the final system of differential equations. The final measured, estimated, and unknown parameters are listed in Table 2.

Table 2: The measured, estimated, and unknown parameters in the final system of differential equations

Measured Values	**Estimated Parameters**	**Unknown Parameters**
$y_{M1}(t)$ $[m]$	k_{s1} $[N/m]$	m_L $[kg]$
$\theta_M(t)$ $[rad]$	k_{d1} $[Ns/m]$	x_L $[m]$
$y_{A1}(t)$ $[m]$	k_{s2} $[N/m]$	
$y_{A2}(t)$ $[m]$	k_{d2} $[Ns/m]$	
d $[m]$	m_0 $[kg]$	
	x_0 $[m]$	

To use the differential equations to solve for the unknown parameters, the position and orientation of the frame, $\widehat{y_{M1}(t)}$ and $\widehat{\theta_M(t)}$, are modeled for the observed wheel centers, $y_{A1}(t)$ and $y_{A2}(t)$, using various combinations of the unknown values, m_L and x_L, and the results are compared to

the measured position and orientation, $y_{M1}(t)$ and $\theta_M(t)$. The combination of unknown values that produces the modeled position and orientation that agrees best with the measured position and orientation are chosen as the best estimates for the unknown values. The error in the position estimation is defined by taking the root mean square of the difference between the measured position, $y_{M1}(t)$, and the estimated position, $\widehat{y_{M1}(t)}$, of the vehicle frame above the front axle as shown in Equation 24. The error in the orientation estimation is defined by taking the root mean square of the difference between the measured orientation ($\theta_M(t)$) and the estimated orientation ($\widehat{\theta_M(t)}$) of the vehicle frame, as shown in Equation 25.

To calculate the total error in the estimation, the position error must be combined with the orientation error. Since the units are different (the position error is in units of meters and the orientation error is in units of radians) the orientation error must be converted from radians into the equivalent error in meters. This is done by simply scaling the orientation error by the distance, d, between the axles. This was determined by calculating the change in position of $y_{M1}(t)$ by a change in orientation $\theta_M(t)$ and use of the small angle approximation. Therefore the total error is defined by Equation 26.

$$E_P = \sqrt{\sum \left(\left(y_{M1}(t) - \widehat{y_{M1}(t)} \right)^2 \right)} \tag{24}$$

$$E_O = \sqrt{\sum \left(\left(\theta_M(t) - \widehat{\theta_M(t)} \right)^2 \right)} \tag{25}$$

$$E_{Avg} = \frac{(E_P + d \cdot E_O)}{2} \tag{26}$$

2.2 Frame Position

In order to use the physics-based suspension response model described in the previous section, the vehicle's frame position and orientation need to be tracked. A custom tracking algorithm was developed to accurately and precisely track regions on the frame of a vehicle using video collected from a side-on view point. The custom tracking algorithm was designed to track a localized region on a vehicle, instead of tracking the entire vehicle. This distinction is critical for the suspension response phenomenology where the movement of the vehicle's frame relative to the vehicle's axle is the observable of interest. The video tracking algorithm developed for this application is optimized to accurately track points on a vehicle traveling through the field-of-view of a stationary camera. For this application, it is assumed that the frame-to-frame movement of the vehicle is small enough to consider the difference in projective distortion between consecutive video frames to be negligible.

The algorithm must be provided a sequence of image frames, and the location, in the first video frame, of the region to track. The region to track is extracted from the first image, and a contrast stretch is applied to remove shallow-gradient edges. Next, the image is converted into a binary edge-image using a Laplacian of Gaussian (LoG) edge detector.[4] The LoG edge detector works by first convolving the input image with a Gaussian kernel to remove high-frequency noise (Equation 27), and then convolving this smoothed response image with a Laplacian gradient operator (Equation 28).[4] The entire process is summarized in Equation 29[4]

$$G(x,y) = \frac{1}{\sqrt{2\pi \cdot \sigma^2}} \cdot exp - \frac{x^2 + y^2}{2 \cdot \sigma^2} \tag{27}$$

$$\Delta G(x,y) = \frac{\partial^2 G}{\partial x^2} + \frac{\partial^2 G}{\partial y^2} \tag{28}$$

$$I_1(x,y) = (I_0(x,y) * G(x,y)) * \Delta G(x,y) \tag{29}$$

where $G(x,y)$ is a symmetric Gaussian kernel, σ is the standard deviation of the Gaussian kernel, $\Delta G(x,y)$ is the Laplacian gradient operator, $I_0(x,y)$ is the input image, and $I_1(x,y)$ is the LoG filtered image. The LoG filtered image, $I_1(x,y)$, is converted to an edge image by finding all of the zero-crossings and setting them equal to one (all other points are zero). An example of this can be seen in Figure 4. Edge-based images were found to be much more reliable for tracking than intensity images, as they produced much sharper responses from the normalized cross-correlation, resulting in reduced false alarms. This binary, edge image becomes the initial template. The next image frame is loaded and a search neighborhood is defined as an n-by-n neighborhood centered at the previous frame's search result. An array of binary edge images is generated using a range of contrast stretches to account for any lighting change. An example of this array is shown in Figure 5. The normalized cross-correlation of the template image and each of the images in the array are calculated using Equation 31[5]

$$\gamma(u,v) = \frac{\Sigma_{x,y}\left[I(x,y) - \overline{I_{u,v}}\right]\left[t(x-u,y-v) - \bar{t}\right]}{\left(\Sigma_{x,y}\left[I(x,y) - \overline{I_{u,v}}\right]^2 \Sigma_{x,y}\left[t(x-u,y-v) - \bar{t}\right]^2\right)^{0.5}} \tag{30}$$

where $I(x,y)$ is the input image, $t(x,y)$ is the template image, $\overline{I_{u,v}}$ is the mean of the input image in the region under the template, and $\bar{t}$ is the mean of the template image. The normalized cross-correlation of the array of images results in an array of intensity images. The magnitude of these

cross-correlation surfaces is going to be highest at the location where the two images align, and the peak response would represent the best match. The highest peak is selected and recorded as the center of the tracked region in the current frame. If no acceptable match is found, the search area is grown by 20 pixels in each of the four directions, and the process is repeated. This continues until an acceptable match is found or the search area becomes too large (for these image sets, the search area was deemed too large when it grew beyond 60 pixels in each direction). The maximum size of an acceptable search will depend on the expected speed of the vehicle and the camera parameters. Once a match is found, it will be used as the new template for the next frame. This is done because the shape of the tracked region will change due to projective distortion as the vehicle travels through the field-of-view of the camera. By continuously updating the template, it was determined that one does not need to account for this projective distortion (assuming the frame-to-frame movement of the vehicle is small). The process is repeated for each subsequent frame using the template selected from the previous frame and continues until no acceptable match is found or the edge of the image is reached.

As a result of continuously updating the template, one needs to track and account for the sub-pixel misalignment that accumulates each time a new template is chosen. If we do not account for this misalignment, the region being tracked can drift away from the true location defined in the first frame. This potential misalignment is tracked by computing the normalized cross-correlation of the new template, and the previous template and then fitting a sub-pixel, two-dimensional Gaussian to the peak. The deviation of the center of the calculated Gaussian from the exact center of the result is the amount of misalignment, which should be less than one pixel along each axis. This misalignment is cumulatively summed from frame-to-frame for each axis, and is compensated for each time the sum reaches an integer pixel deviation by shifting the current template. This is done

for both the x and y axis. Figure 6 illustrates the cumulative drift that can occur, and effectiveness of the drift mitigation.

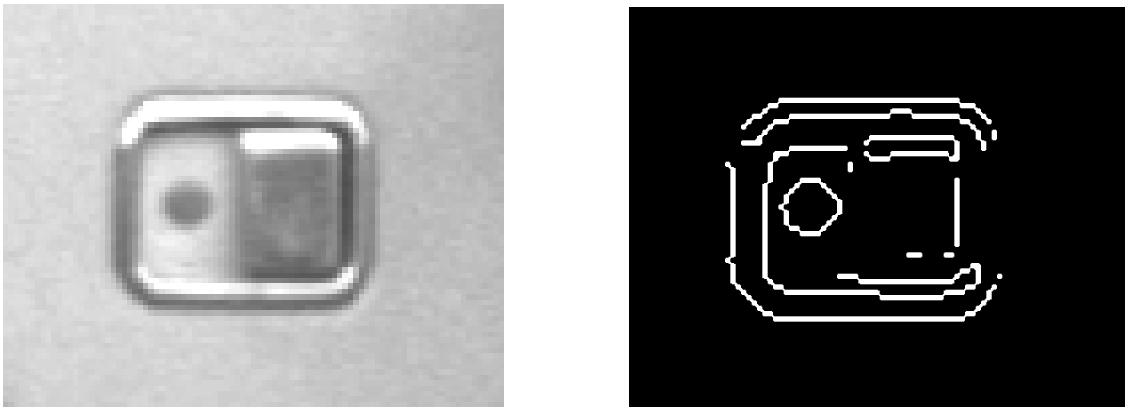

(a) (b)

Fig 4: The region to track (4a) and a edge image of the region to track (4b)

(a) (b) (c)

Fig 5: An array of binary, edge images generated by varying the contrast stretch from mild contrast stretch (5a) to severe contrast stretch (**??**)

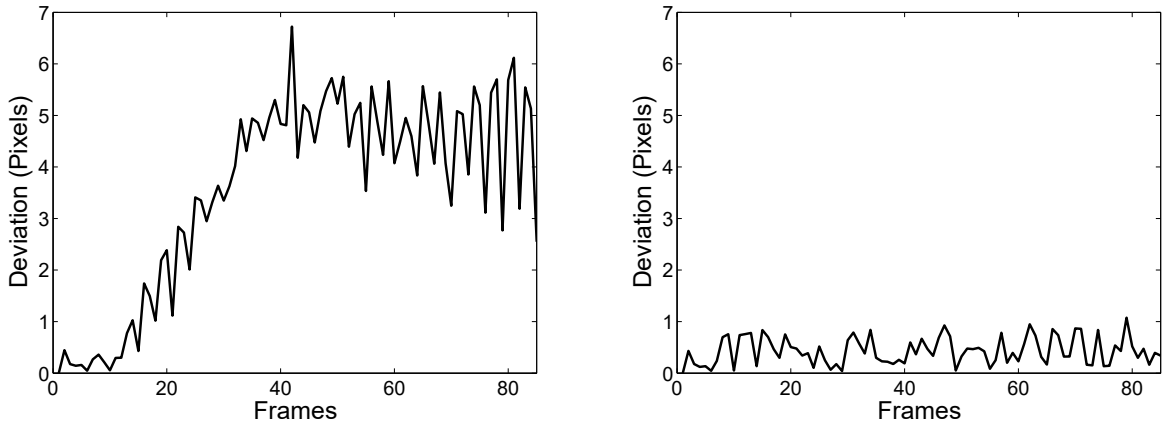

(a) (b)

Fig 6: The amount of tracking drift in pixels without the drift correction (6a) and with the drift correction (6b)

2.3 Wheel Position

The final measurement needed to use the physics-based suspension response model described earlier is the position of the vehicle's wheel centers, which will be used as the road profile. A custom tracking algorithm was developed to accurately and precisely track the center of a vehicle's wheels using video collected from a side-on view point. This algorithm was designed to track the center point of a wheel traveling through the field-of-view of the camera. The algorithm must be provided with a sequence of image frames, and the location, in the first video frame of the wheel to track. A region around the wheel is selected from the first image, and a contrast stretch is applied to remove shallow-gradient edges. Next, the region is converted into a binary image by thresholding. Each connected region in the binary image is identified using flood-fill based algorithm.[6] The small regions are removed from the binary image based on a size threshold. Regions not fully contained by the area of interest (regions that touch the edge) are also removed. The convex hull is then calculated and the area within it is filled. A LoG edge detector is applied. This results in a set of points making up the perimeter of the region. These points are fit to the quadratic equation for an ellipse (Equation 31) using a linear least squares method and the residual error from the least squares method is calculated.

$$Ax^2 + 2Bxy + Cy^2 + 2Dx + 2Fy + G = 0 \tag{31}$$

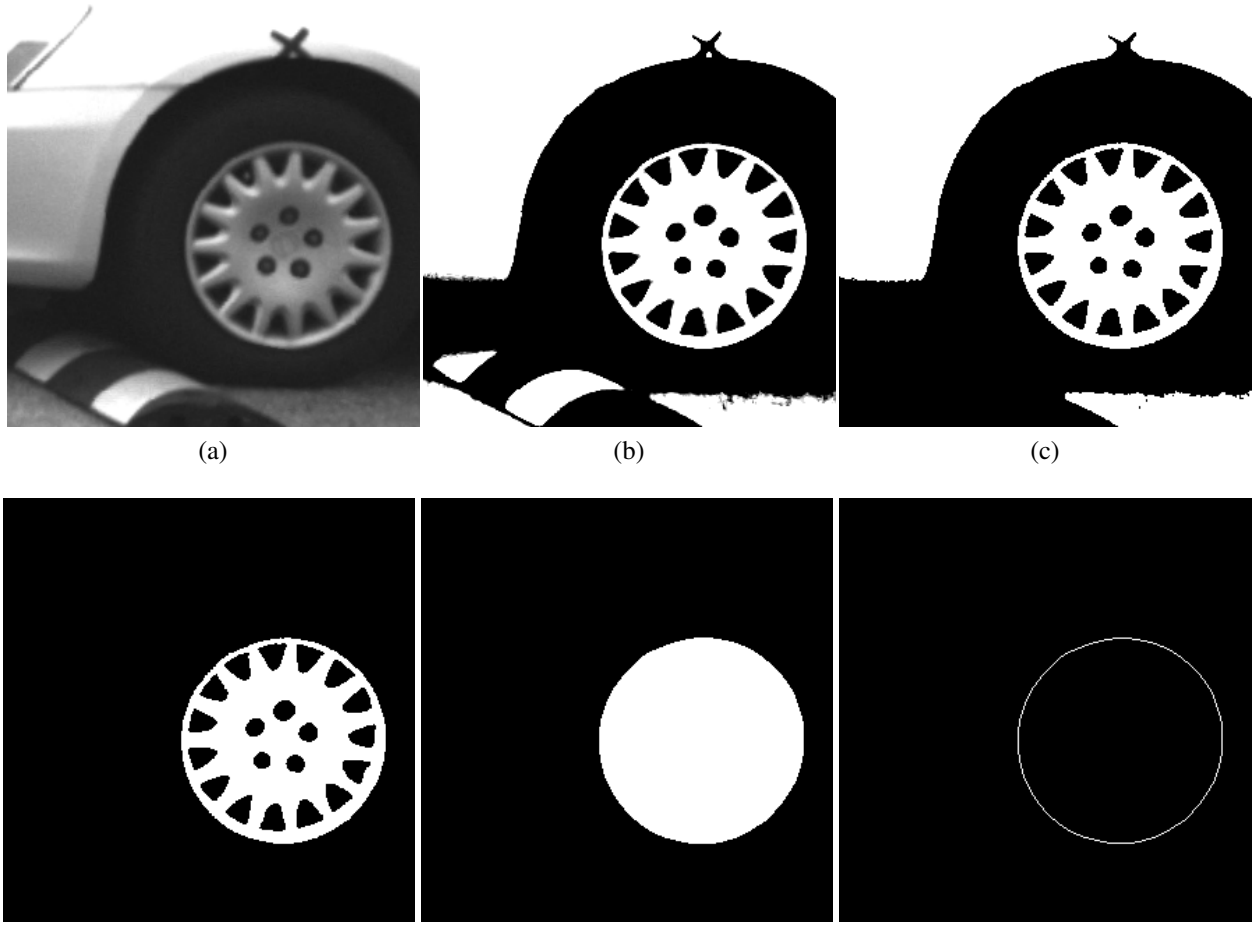

(a) (b) (c)

(d) (e) (f)

Fig 7: Contrast stretched image (7a), thresholded (7b) , small regions removed (7c), edge regions removed (7d), convex hull applied (7e), edge detector applied(7f)

This process is repeated for a range of contrast stretches and the region with the lowest residual error (most elliptical) is selected as the best estimate for the wheel. If no acceptable match is found, the area of interest is increased in size and the process is repeated. Once an acceptable wheel estimate is found, the center of the region is calculated and the process is repeated for the next video frame using a region of interest defined as a box around the wheel center from the previous frame.

Once the axle position has been tracked across the field of view of the video camera a Gaussian-like function is fit to the measured data. This is done so the vertical position of each axle center

can be expressed in closed-form which is a requirement of the differential equation solver used for this application. The Gaussian-like function that was found to best fit most axle data as the vehicle traveled over a speed bump is

$$y_{A1}(t) = H \cdot \exp\left(-\frac{(t-t_0)^4}{2 \cdot c^4}\right) \tag{32}$$

where H is the maximum height the wheel center reaches, t_0 is the time when the wheel center reaches its peak, and c is a parameter that determines the wideness of the function. To find the parameters that best fit the measured data, MATLAB's unconstrained multivariable optimization routine, 'fminunc' was used. This routine was configured to use the Broyden[7]Fletcher[8]Goldfarb[9]Shanno[10] (BFGS) algorithm. Once the optimal values for the parameters (H, t_0, and c) were found, the closed form expression was used to describe the vertical position of the front and rear axles.

3 Results

A full-scale field test was carried out to test the validity of the method, and the practicality of the remote sensing techniques. The test was carried out at the Savannah River Site, a United States Department of Energy facility located in Aiken, South Carolina. The test used a 2006 Honda Accord in three load conditions; the recommended maximum load, half the recommended maximum load, and no load. A minimum of three test runs were completed for each load condition. The test utilized an ARRIFLEX D-21 high-resolution cinematic style video camera positioned adjacent to the path of the vehicle to collect 30 frames-per-second video at a resolution of 2880-by-1620 as the test vehicle traveled over a speed bump.

For each test run, the video data was processed using the methods described in the previous

section and resulted in frame position, and wheel center positions as a function of time. An example of a processed dataset from the second field test can be seen in Figure 8.

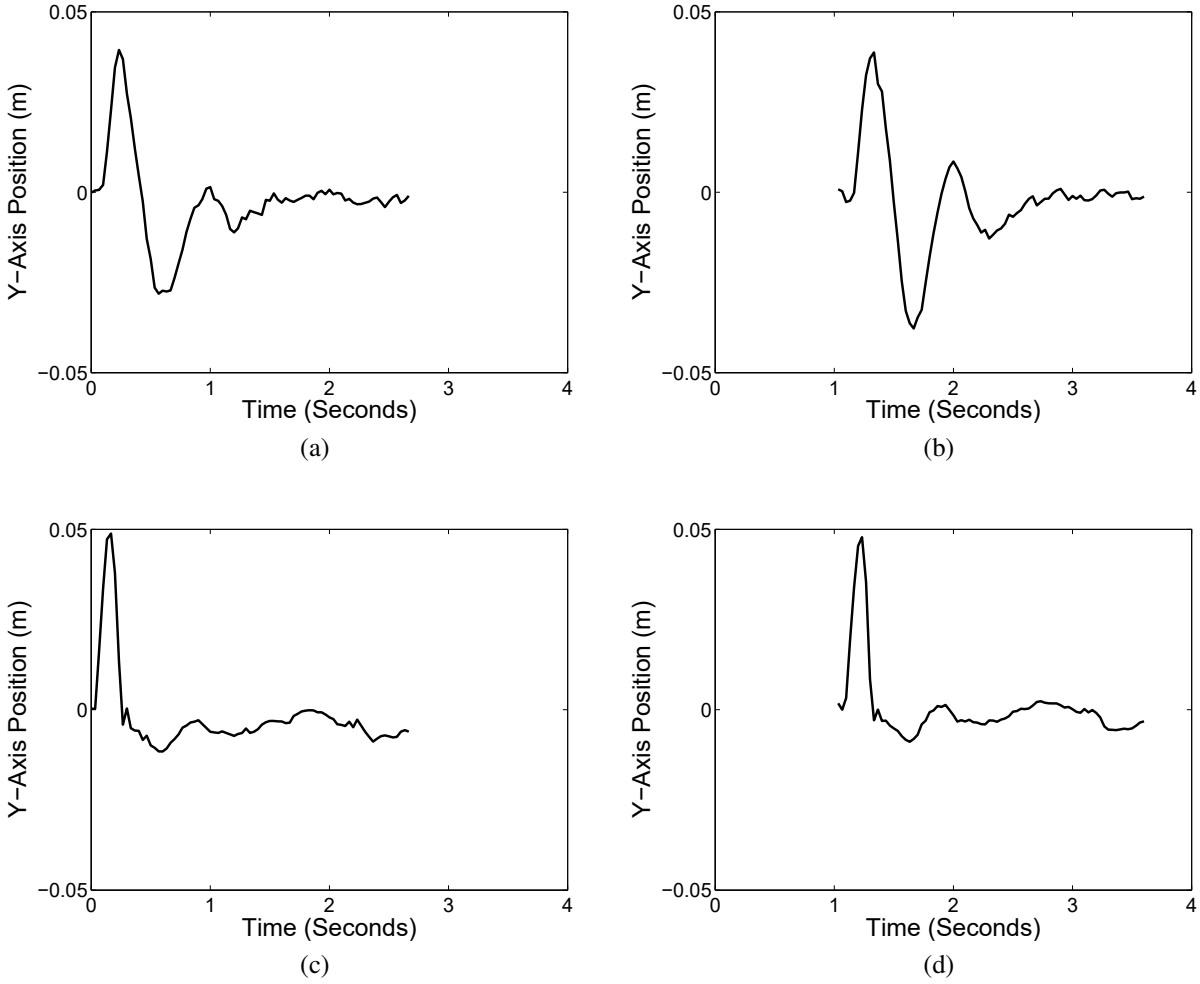

Fig 8: An example of the vertical front frame position (8a), rear frame position (8b), front wheel center (8c), and rear wheel center (8d) extracted from the video data.

For each data set, the model described in Section 2.1 was used to generate nearly 250,000 simulations for each test run. Each simulation used a different combination of vehicle load mass and vehicle load center of gravity. Each simulation used the same best-fit Gaussian-like approximation of the tracked wheel centers as inputs, and used the vehicle and suspension parameters seen in Table 3. Where m_0 is the unloaded mass of the vehicle, x_0 is the x-axis distance of the vehicle's

center of gravity from the front wheel center (positive means towards the rear of the vehicle), J_0 is the moment of inertia of the unloaded vehicle, k_{s1} is the front suspension spring constant, k_{d1} is the front suspension damping coefficient, k_{s2} is the rear suspension spring constant, and k_{d2} is the rear suspension damping coefficient. All of these parameters are required to be known for this method of analysis to be possible. The only parameters allowed to vary during the simulations were the mass of the load, and the center of gravity of the load. The load mass array ranged from 0 to $600\,\mathrm{kg}$ at step sizes of $2.7\,\mathrm{kg}$ and the center of gravity array ranged from 0 to $5\,\mathrm{m}$ at step sizes of $0.01\,\mathrm{m}$. Each generated frame response was compared to the measured frame response, and three error values were calculated for each simulation based on the error equations from Section 2.1. The frame position error, which characterized how well the model fit the y-axis position of the front frame position, the orientation error, which characterized how well the model fit the frame rotation, and the average error, which combined the position and orientation errors. Heat map representations of the averaged error can be seen in Figure 9. It should be noted that it took extensive research and brute force calculations to find valid suspension parameters for this test vehicle. Future work should employ field testing to measure the suspension parameters, or enlist the support of manufacturers to generate the required database of suspension response values.

Table 3: Table of passenger vehicle parameters

Vehicle Parameter	**Value**
m_0	$1430\,\mathrm{kg}$
x_0	$1.4\,\mathrm{m}$
J_0	$2261\,\mathrm{kg\,m^2}$
k_{s1}	$53{,}306\,\mathrm{N/m}$
k_{d1}	$3555\,\mathrm{N\,s/m}$
k_{s2}	$104{,}640\,\mathrm{N/m}$
k_{d2}	$4465\,\mathrm{N\,s/m}$

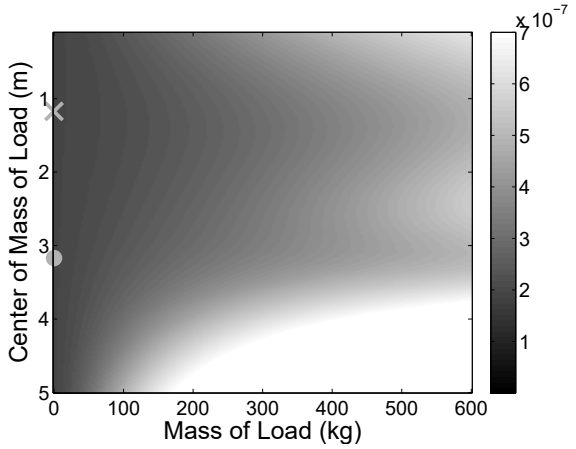

(a) Frame position error heat map for the unloaded car

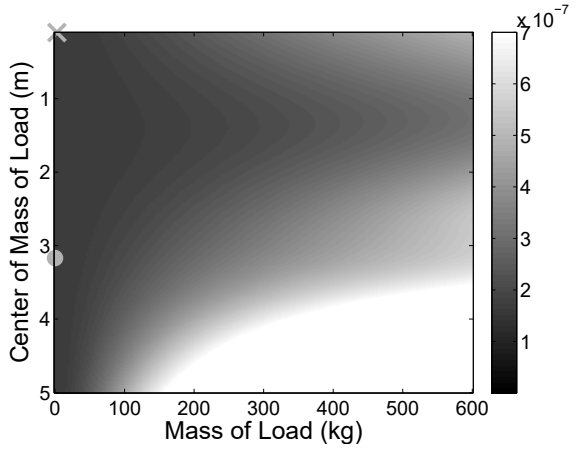

(b) Frame orientation error heat map for the unloaded car

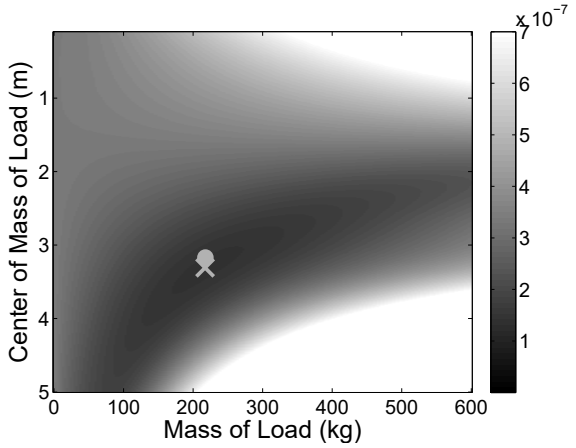

(c) Frame position error heat map for the half loaded car

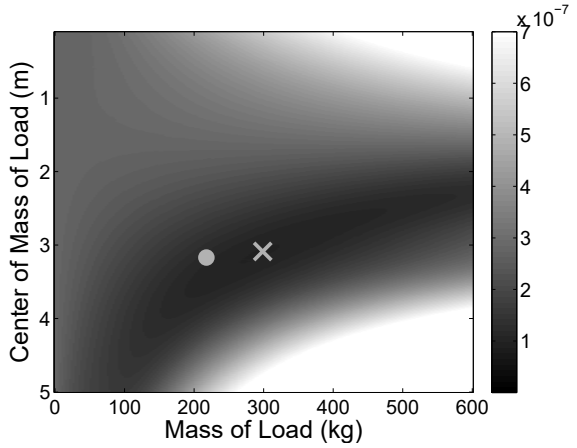

(d) Frame orientation error heat map for the half loaded car

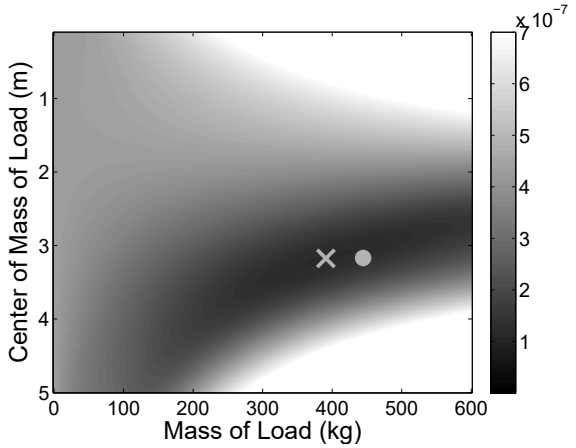

(e) Frame position error heat map for the fully loaded car

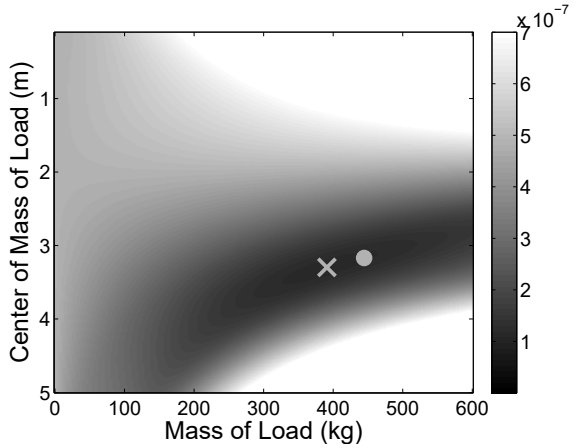

(f) Frame orientation error heat map for the fully loaded car

Fig 9: Frame position and orientation error heat maps for the unloaded, half-loaded, and fully-loaded test vehicle. The circle represents the true value, and the X represents the measured value.

4 Conclusions

Remotely-collected video was used to calculate the vertical position of the vehicle's axles, the vertical position of the vehicle's frame, and the angular orientation of the vehicle's frame over time as the vehicle traveled over a speed-bump. These signals were used to calculate the mass and center of gravity of the vehicle's load using the method described in Section 2.1. The results from the field test (Figure 9) show strong agreement between the calculated and true load mass and center of gravity. The only major disagreement was in the location of the center of gravity for the unloaded vehicle. This disagreement is inconsequential, as a mass of zero does not have a center of gravity.

The results of this testing were very positive, however there are areas in which improvements could be made. First, it is critical to understand the variability of the estimated vehicle parameters by vehicle class, make, and model. For this method to be accurate, a system would need to be in place to classify each vehicle and predict the required vehicle parameters based on this classification. It is currently unclear as to how extensive this classification system would need to be. For this method to be effective, the video camera needs to observe the front-most and rear-most axles of the vehicle simultaneously from a time just prior to the vehicle reaching the speed-bump until approximately three seconds after the last axle travels over the speed bump. Additionally, the minimum measurement resolution (based on the vehicle modeled in this study) is approximately two millimeters. Depending on the length, and the speed of the vehicle these requirements may not be achievable using a single video camera, but instead two synchronized video cameras may be required.

Acknowledgments

The authors would like to thank the United States Department of Energy, National Nuclear Security Administration, Office of Defense Nuclear Nonproliferation (NA-22) for their support of this work under contract number DE-AC09-08SR22470/AC799980. Special thanks are expressed to Dr. Alfred Garrett, Dr. David Coleman, and Dr. Larry Koffman of the Savannah River National Laboratory for their invaluable assistance in facilitating the field experiments carried out in Aiken, South Carolina.

References

1 B. Jacob and V. Feypell-de La Beaumelle, "Improving truck safety: Potential of weigh-in-motion technology," *IATSS Research* **34**(1), 9–15 (2010).

2 B. Taylor, A. Bergan, N. Lindgren, and C. B. P. D. P. Eng, "The importance of commercial vehicle weight enformcement in safety and road asset management," *Annual Review pp* **234**, 237 (2000).

3 K. Helmi, T. Taylor, and F. Ansari, "Shear force–based method and application for real-time monitoring of moving vehicle weights on bridges," *Journal of Intelligent Material Systems and Structures* **26**(5), 505–516 (2015).

4 D. Marr and E. Hildreth, "Theory of edge detection," *Proceedings of the Royal Society of London B: Biological Sciences* **207**(1167), 187–217 (1980).

5 J.-C. Yoo and T. H. Han, "Fast normalized cross-correlation," *Circuits, Systems and Signal Processing* **28**(6), 819–843 (2009).

6 P. Soille, *Morphological image analysis: principles and applications*, Springer Science & Business Media (2013).

7 C. G. Broyden, "The convergence of a class of double-rank minimization algorithms 1. general considerations," *IMA Journal of Applied Mathematics* **6**(1), 76–90 (1970).

8 R. Fletcher, "A new approach to variable metric algorithms," *The Computer Journal* **13**(3), 317–322 (1970).

9 D. Goldfarb, "A family of variable-metric methods derived by variational means," *Mathematics of Computation* **24**(109), 23–26 (1970).

10 D. F. Shanno, "Conditioning of quasi-newton methods for function minimization," *Mathematics of Computation* **24**(111), 647–656 (1970).

Troy R. McKay received his BA in Applied Physics from SUNY Geneseo in 2003, and his MS from SUNY Buffalo in Electrical Engineering in 2007. He received his PhD in Imaging Science from the Rochester Institute of Technology in 2016. He is currently the founder and President of Hyperspectral Solutions, LLC.

Carl Salvaggio received his BS and MS degrees in Imaging Science from the Rochester Institute of Technology (RIT) in 1987. He received his PhD in Environmental Resource Engineering in 1994 from the State University of New York, College of Environmental Science and Forestry, at Syracuse University. From 1994 to 2002, he worked on model validation and database development for the defense intelligence community. Since 2002 he has been a professor of Imaging Science at RIT.

Jason W. Faulring earned his BS in Computer Engineering from the Rochester Institute of Technology (RIT) in 2003. As a senior systems engineer at RIT's remote sensing laboratory from 2003 to 2015, he developed novel airborne and ground-based sensing systems for the lab's research efforts. He is currently a senior engineer and partner at AppliedLogix, LLC developing custom hardware and software solutions.

Glenn D. Sweeney received his BS degree in Imaging Science from the Rochester Institute of Technology in 2013, and his MSc in Color Science from the CIMET University consortium in 2015. After graduation he has entered the workforce designing image quality test equipment for mobile camera systems.

List of Figures

1 Simplified suspension diagram for a standard two-axle vehicle

2 Example of the front axle traveling over a rise in the road (speed bump)

3 Example of the completely unloaded vehicle traveling over flat road (both springs are in the uncompressed state)

4 The region to track (4a) and a edge image of the region to track (4b)

5 An array of binary, edge images generated by varying the contrast stretch from mild contrast stretch (5a) to severe contrast stretch (**??**)

6 The amount of tracking drift in pixels without the drift correction (6a) and with the drift correction (6b)

7 Contrast stretched image (7a), thresholded (7b) , small regions removed (7c), edge regions removed (7d), convex hull applied (7e), edge detector applied(7f)

8 An example of the vertical front frame position (8a), rear frame position (8b), front wheel center (8c), and rear wheel center (8d) extracted from the video data.

9 Frame position and orientation error heat maps for the unloaded, half-loaded, and fully-loaded test vehicle. The circle represents the true value, and the X represents the measured value.